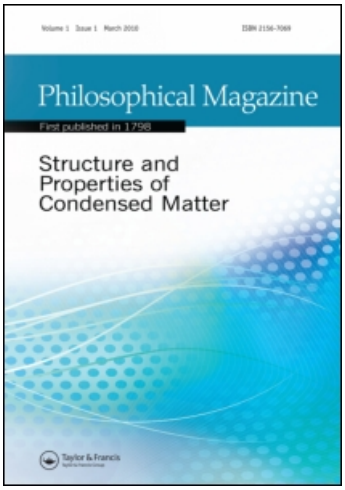

Philosophical Magazine
Publication details, including instructions for authors and subscription information:
http://www.informaworld.com/smpp/title~content=t713695589

Kinetics and dynamics of frictional stick-slip in mesoscopic boundary lubrication

O. M. Braun[a]; Erio Tosatti[bcd]
[a] Institute of Physics, National Academy of Sciences of Ukraine, 03028 Kiev, Ukraine [b] International School for Advanced Studies (SISSA), I-34014 Trieste, Italy [c] CNR-INFM Democritos National Simulation Center, I-34014 Trieste, Italy [d] International Centre for Theoretical Physics (ICTP), I-34014 Trieste, Italy

First published on: 03 May 2011

To cite this Article Braun, O. M. and Tosatti, Erio(2011) 'Kinetics and dynamics of frictional stick-slip in mesoscopic boundary lubrication', Philosophical Magazine,, First published on: 03 May 2011 (iFirst)
To link to this Article: DOI: 10.1080/14786435.2011.575410
URL: http://dx.doi.org/10.1080/14786435.2011.575410

Philosophical Magazine
2011, 1–23, iFirst

Taylor & Francis
Taylor & Francis Group

Kinetics and dynamics of frictional stick-slip in mesoscopic boundary lubrication

O.M. Braun[a]* and Erio Tosatti[bcd]

[a]*Institute of Physics, National Academy of Sciences of Ukraine, 46 Science Avenue, 03028 Kiev, Ukraine;* [b]*International School for Advanced Studies (SISSA), Via Beirut 2-4, I-34014 Trieste, Italy;* [c]*CNR-INFM Democritos National Simulation Center, Via Beirut 2-4, I-34014 Trieste, Italy;* [d]*International Centre for Theoretical Physics (ICTP), P.O. Box 586, I-34014 Trieste, Italy*

(*Received 24 January 2011; final version received 23 March 2011*)

The kinetics and dynamics of frictional stick-slip motion of a slider of size extending from mesoscopic upward is analyzed within the framework of a multi-contact, earthquake-like model. The microscopic contacts are characterized by a distribution of static thresholds for individual breaking. The condition for an overall elastic instability leading to stick-slip sliding are derived and details of the slip motion are studied theoretically. The crucial model parameters emerging from this analysis include the delay time for each micro-contact to reform after breaking, the strength of elastic interaction between the contacts, the elasticity of contacts and of the slider, and the distribution of static thresholds for their breaking. The dynamics is also studied with the help of a scaling procedure. As a prototype application, we adopt parameters appropriate to describe recent surface force apparatus (SFA) boundary lubrication experiments. Despite suggestions of extremely large lubricant viscosities, the experimental data are shown to be fully compatible with ordinary, bulk-like viscosity values once the multi-contact aspects are taken into account.

Keywords: boundary lubrication; nanotribology; viscosity; stick-slip

1. Introduction

Friction, one of the oldest, physically rich, and practically most relevant problems, is in several important aspects still not fully understood. We concentrate here on friction in conditions of boundary lubrication, when the sliding occurs without wear or plastic deformation of the sliding surfaces, with a molecularly thin lubricant film in between. It is well established that liquids confined to films thinner than five to eight monolayers become layered and solid-like, so that the shearing of the film is associated with a nonzero yield stress [1,2]. Perhaps because of that, a widespread opinion is that the viscosity of the thin confined lubricant film is many orders of magnitude higher than the bulk viscosity. Also, the experimentally observed critical velocities of the transition from stick-slip to smooth sliding are over 10^6 times smaller than that observed in molecular dynamics (MD) simulations. Although this last

*Corresponding author. Email: obraun.gm@gmail.com

ISSN 1478–6435 print/ISSN 1478–6443 online

DOI: 10.1080/14786435.2011.575410
http://www.informaworld.com

point had been resolved with the help of earthquake-type models [2,3], the question whether there is indeed evidence of an abnormally large viscosity of the confined lubricant fluid still remains unclear. In a recent paper, Klein [4] presented remarkable surface force balance (SFB) studies of stick-slip friction across molecularly thin film of octamethylcyclotetrasiloxane (OMCTS). This data is especially important since SFB is quantitatively accurate, with a well-defined contact region between molecularly smooth solid mica surfaces. Klein showed that a straightforward fitting of the time dependence of the slider coordinate $X(t)$ during slip in the form $M\ddot{X} + M\tilde{\eta}\dot{X} = K(v_d t - X)$, where M is the slider mass, K is the setup rigidity and v_d is the driving velocity, yields a value for the boundary fluid lubricant viscosity $\tilde{\eta}$ about 10^4 times higher than that expected from the bulk viscosity of fluid OMCTS. Claims of a factor 10^6 or even larger between boundary lubricant and bulk lubricant viscosities had been made earlier on similar grounds [5,6], but had not been physically substantiated. Recently Bureau [7] declared a lower factor 10^2 for the same system, still too high to be reasonably explained. To be sure, the case of a monolayer or bilayer confined between two planar surfaces is extreme and the fluid film properties are understandably far from their bulk counterparts [2,8]; but already a three-layer film, once melted during slips, should exhibit properties not very different from the bulk ones, as is found in essentially all MD simulations [1,2]. A crucial point here is that many simplified schematizations treating large systems of mesoscopic and macroscopic size as though they were microscopic and homogeneous are unjustified and may lead to misleading conclusions.

The aim of this work is to formulate and numerically simulate a scheme capable of addressing boundary lubricated sliding from the mesoscale upward. On sufficiently large length-scales the thin lubricant film, if not the sliding surfaces themselves, can hardly be expected to remain homogeneous and uniform. Typically, the initially solid lubricant film will consist of domains with different orientation or structure, characterized by different yield stresses; it is therefore unreasonable to assume that a mesoscopic or macroscopic lubricant film should melt and begin sliding uniformly as a whole. Rather, different domains will generally start sliding one by one, at different stress values. Systems of this type have been first described with an earthquake-like model [9]. The scope of the present work is to show that, once the proper parameters are identified and chosen, this approach describes very well the lubricated sliding features of the surface force apparatus/surface force balance (SFA/SFB) boundary observed experimentally. This modeling suggests further simple experiments which could test our proposition. A preliminary version of this work has been published as a short letter [10].

Our work is based on the time-honored earthquake-like (EQ-like) model, developed from the original Burridge–Knopoff model [3,9–17]. Persson [13] was the first to adjust the EQ model to sliding friction and describe qualitatively the stick-slip and smooth sliding regimes observed in laboratory experiments. Yet, Persson's model, being one-dimensional, cannot reproduce quantitatively all experimental aspects. Extension of the model to two dimensions [3] improved the agreement with experiments, addressing in particular the critical velocity of the transition from stick-slip to smooth sliding. Successively however [15,16], it became clear that an important ingredient not previously appreciated is the distribution of static (yield) thresholds. For the sake of simplicity in the previous variants of the model,

all contacts were assumed to be identical, and the distribution of thresholds therefore entered only implicitly through temperature fluctuations [13] or interaction between the contacts [3]. However, proper incorporation from the very beginning of a threshold distribution allows us to identify analytically the steady state solution of the EQ model and to identify the conditions for the elastic instability which is the necessary condition for the stick-slip to appear [18].

In this paper, we use the EQ-like model to describe mesoscopic boundary lubrication with the following goals:

(i) to describe the slip dynamics in detail in the presence of multi-contact inhomogeneity;
(ii) to consider the effect of elastic interactions between the contacts;
(iii) to consider the real dynamics of sliding contacts with the help of molecular dynamics, highlighting the difference between that and predictions of the EQ algorithm;
(iv) to consider the effects of elasticity of the sliders.

The paper is organized as follows. The model is described in Section 2. The model parameters appropriate to SFA/SFB boundary lubrication experiments are discussed and determined in a separate Section 3. The kinetics of the model is studied in detail in Section 4, while its dynamics is considered in Sections 5, 6 and 7. Comparison of simulation results with the SFB boundary lubrication experiments is presented in Section 8, and Section 9 summarizes our results and conclusions.

2. Model

Our chosen EQ-like model is shown schematically in Figure 1. Let there be N "contacts" (asperities, domains, regions, etc.) that couple the bottom immobile substrate (the base) with the top substrate (the slider). All contacts are attached to the bottom substrate through springs of elastic constants k_i, $i = 1, 2, \ldots, N$. The contacts are arranged in a perturbed 2D lattice (in simulation we first arrange contacts at the regular sites of a triangular lattice of spacing a, and then randomly shift them off the lattice by Δx_i and Δy_i, where Δx_i, Δy_i are small Gaussian random displacements with zero mean and standard deviation Δx). This procedure gives the unstressed positions of contacts $r_{i;0} = (x_{i;0}, y_{i;0})$. When the system evolves, the contact

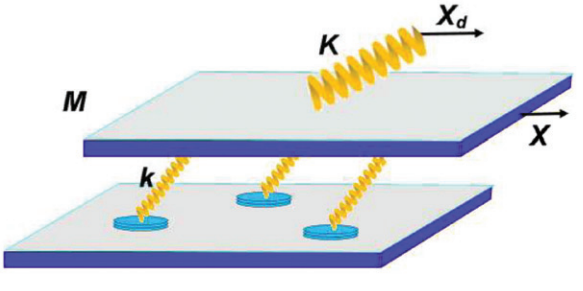

Figure 1. The earthquake-like model.

positions change from $r_{i;0}$ to $r_i=(x_i, y_i)$, where $x_i=x_{i;0}+l_{xi}$, $y_i=y_{i;0}+l_{yi}$, and l_{xi} and l_{yi} are the stretchings (relative to the bottom substrate) of the ith contact along x and y directions respectively. The spring force which acts on the ith pinned contact from the bottom substrate is $f_{xi}^{(\mathrm{sub})}=-k_i l_{xi}$. We consider in addition a pairwise elastic interaction between contacts, described by the potential $V(r)=g/r^3$, where g is a constant [19,20]. Therefore, the force acting on the ith contact from its nearest neighbors (NNs) is equal to $f_{xi}^{(\mathrm{int})}=-\sum_{j\,(j\neq i)}^{\mathrm{NN}}\partial V(x_j-x_i)/\partial x_i=3g\sum_{j\,(j\neq i)}^{\mathrm{NN}}(x_i-x_j)/r_{ij}^5$; in simulation we assume approximately that inside this formula $r_{ij}\approx r_{ij;0}=[(x_{i;0}-x_{j;0})^2+(y_{i;0}-y_{j;0})^2]^{1/2}$. The total force acting on the pinned contact from its NNs and from the top substrate (the slider) is $f_{xi}=f_{xi}^{(\mathrm{sub})}+f_{xi}^{(\mathrm{int})}$ (f_{yi} is defined in the same way).

We let the contacts couple "frictionally" with the slider in the following sense. As long as the total force magnitude on the contact $f_i=(f_{xi}^2+f_{yi}^2)^{1/2}$ is below a threshold value f_{si}, the contact moves together with the slider. When the force exceeds the threshold, the contact detaches from the slider and slides relative to the top substrate for some time τ_i after which the contact sliding stops as it attaches again to the slider. During its sliding the contact experiences a drag force from the slider $f_{xi}^{(\mathrm{drag})}=m_i\eta_i[v_{sx}-\mathrm{d}l_{xi}(t)/\mathrm{d}t]$ (and similarly defined $f_{yi}^{(\mathrm{drag})}$), where $v_{sx}(t)$ and $v_{sy}(t)$ are the two components of the slider velocity, m_i is the effective mass of the contact and η_i is a corresponding damping coefficient. After the time τ_i, the contact attaches again to the slider, and its stretching is determined from the condition that the total force f_i on the contact is equal to the backward threshold force f_b [2].

The four parameters f_{si}, m_i, k_i, and η_i characterize each contact. We assume the thresholds f_{si} to take random values from a Gaussian distribution of mean value f_s and standard deviation Δf_s,

$$P_G(f_{si};f_s,\Delta f_s)=\frac{1}{\Delta f_s\sqrt{2\pi}}\exp\left[-\frac{1}{2}\left(\frac{f_{si}-f_s}{\Delta f_s}\right)^2\right]. \tag{1}$$

In simulation, the distribution of thresholds $P_c(f)$ is defined on the interval $0<f<f_m$, where $f_m\gg f_s$ so that we use the corrected distribution $P_c(f)=\mathcal{N}\{P_G(f)-P_G(0)-(f/f_m)[P_G(f_m)-P_G(0)]\}$, where $\mathcal{N}$ is the normalization constant, so that $P_c(f)$ satisfies the condition $P_c(0)=P_c(f_m)=0$ [17]. In principle, both f_{si} and m_i should be proportional to the contact area $A_i=\pi a_i^2$ (a_i is the contact radius). The contact's stiffness is given by $k_i\approx\rho c^2 a_i$ (see [13] and Appendix A in Ref. [17]), where ρ is the mass density and c is the transverse sound velocity of the material which forms the contacts. Reasonably, we take $m_i=mf_{si}/f_s$ and $k_i=k(f_{si}/f_s)^{1/2}$, where m and k are the mean mass and stiffness of the contacts. When a contact is "reborn" we assign new values to its parameters. The viscosity parameter η_i is assumed to be the same for all contacts, for example the bulk viscosity coefficient of the lubricant as discussed below in Section 3.

The macroscopic slider, modeled as a solid body of mass M, experiences a force F_B from all contacts as described above (i.e. $\vec{F}_B$ is the sum $\sum_i^N\vec{f}_i$ of the forces from the pinned contacts, plus the sum of drag forces from the sliding contacts). In addition, it is externally driven through a spring of elastic constant K pulled with velocity v_d. Because the slider is solid, any abrupt events, e.g. the onset or stopping of sliding, will excite vibrations with the setup frequency $\Omega_S=(K/M)^{1/2}$;

if undamped, these vibrations would disturb the results. In a real system, such oscillations are damped due to internal friction within the slider setup. To incorporate that effect, we introduce a viscous damping coefficient η_S relative to its average velocity, so that the slider motion is described by the equation

$$M\ddot{X} + M\eta_S\big(\dot{X} - \langle\dot{X}(t)\rangle\big) = F_B(t) + K(X_d - X), \tag{2}$$

where $X_d = v_d t$ and

$$\langle\dot{X}(t)\rangle = \eta_S \int_{-\infty}^{t} \mathrm{d}t'\, \dot{X}(t')\, e^{-\eta_S(t-t')}, \tag{3}$$

and similar equations for the Y coordinate of the slider.

Our simulation is conducted with two separate algorithms: the EQ (earthquake) algorithm, typical for cellular automata models, and the MD (molecular dynamics) algorithm, where the atomistic dynamics of contacts is simulated. The EQ algorithm, which ignores the microscopic dynamics of contacts, assumes that a contact remains in the detached state for a "delay" time $\tau_i = \tau_d$, where τ_d is a parameter of the model.

In the MD algorithm, we assume that the detached contact moves until the absolute value of its velocity (relative to the slider) reduces below the value $v_b = f_b/m_i\eta_i$ and, at the same time, the total force acting on the contact is lower than f_b. In more detail, the contact is re-attached back to the slider as soon as $f_i^2(t) + |\vec{f}_i^{\,(\mathrm{drag})}(t)|^2 \le f_b^2$. To estimate the contact sliding time, which we denote as τ_c, let us consider its motion. When the contact detaches, it moves according to the equation $\ddot{l} + \eta\dot{l} + (k/m)l = \eta v$. Its solution is $l(t) = \Delta l + (l_R\cos\widetilde{\omega}t - l_I\sin\widetilde{\omega}t)e^{-\lambda t}$, where $\Delta l = m\eta v/k$, $l_R = l(0) - \Delta l$, $l_I = -\lambda l_R/\widetilde{\omega}$, $\lambda = \eta/2$, and $\widetilde{\omega} = (k/m - \eta^2/4)^{1/2}$ (we assume that the contact's motion is not overdamped, so that $\widetilde{\omega} > 0$). This gives $\tau_c \approx \eta^{-1}\ln[l(0)\widetilde{\omega}/v_{\min}]$, where $v_{\min} \sim 1\text{–}10\,\mathrm{m\,s^{-1}}$ is the minimal velocity for smooth motion of a contact over a substrate [2,21]. This estimate leads to $\tau_c \sim 10^{-11}\,\mathrm{s}$ (since $\eta \sim 10^{11}\,\mathrm{s^{-1}}$, and the logarithmic factor does not change the order of magnitude), a value which is negligibly small relative to characteristic times of the system. The total delay time τ_i however should include, in addition to the real sliding time τ_c, the time τ_f needed for formation (re-solidification) of the contact, so that $\tau_i = \tau_c + \tau_f$. The time τ_f is generally macroscopic and is a parameter of our model as further discussed below.

3. Parameters

The model parameters are chosen in the following way, mainly bearing in mind the SFA/SFB (surface force apparatus/balance) for boundary lubrication experiment [4]. The number of contacts could be taken anywhere between $N \sim 10^2$ and 10^5 [1,2]; this parameter is not crucial provided $N \gg 1$. The mass of the slider M and its rigidity K are defined by the experimental setup to be discussed further below. The damping η_S is also determined by the setup and can be measured experimentally; typically it should be of the order $\eta_S \sim 0.1\,\Omega_S$. The driving velocity v_d is defined by experimental conditions and is of the order of $\mu\mathrm{m\,s^{-1}}$ typically. The mean distance between the contacts may be found as $a = (A/N)^{1/2}$, where A is the "visible" contact area; reasonable values are $a \sim 1\text{–}10^3\,\mu\mathrm{m}$ [1,2].

The delicate point here is to assign microscopic parameter values f_{si}, m_i, k_i, and η_i of the individual contacts. The threshold force f_s can in principle be found with the help of large-scale MD simulation, if the area of the contact A_i (or its linear size $a_i = (A_i/\pi)^{1/2}$) is known; the latter may be measured experimentally by optical methods ($A_i \sim A/N$ for SFB experiments with mica surfaces, and $A_i \ll A/N$ for a contact of rough surfaces). Also f_s may be estimated from the yield stress $P_{\text{yield}} \approx f_s/A_i$ (typically $P_{\text{yield}} \sim 10^5$–$10^8\,\text{N m}^{-2}$). However, the simplest solution is to take this value from the experiment as $f_s = F_s/N$, where F_s is the measured maximal spring force ($F_s = \mu_s F_l$, where $\mu_s \lesssim 1$ and F_l is the load). The ''backward'' force f_b is, as follows from MD simulations [2], of the order of $f_b \sim (0.01$–$0.1) f_s$ (again, this parameter is not crucial). A value of the contact stiffness k can be estimated as $k \approx \rho c^2 a_i$ [10,13,17]. We expect the total stiffness of the sliding interface to be higher than the setup stiffness, $Nk \gg K$.

The mass of the contact can be estimated as $m \approx \rho a_i^3$ for the contact of rough surfaces, or as $m = A_i h \rho$ for the lubricating film, where ρ is the mass density of the material which forms the contacts (i.e. of the substrate or of the lubricant correspondingly) and h is the film thickness. The coefficient η defines the damping of the contact motion relative to the slider and takes values of the order of $\eta \sim 10^{11}$–$10^{12}\,\text{s}^{-1}$ (for phononic damping $\eta \sim (0.01$–$0.1)\omega_0$, where ω_0 is a characteristic frequency of the substrate, e.g. the Debye frequency). For the lubricating film, the value of η can be linked with the bulk viscosity $\tilde{\eta}_{\text{bulk}}$ by the relation $\eta = \tilde{\eta}_{\text{bulk}}/\left(h^2\rho\right)$ as follows from the equation for the drag force, $m\eta v = \tilde{\eta}_{\text{bulk}} A_i v/h$. Both the mass m and the damping η play a role in MD evolution of contacts, while in the EQ algorithm they determine the drag force only.

The elastic interaction between the contacts becomes important when $g/a^3 \sim f_s a$; therefore, it is interesting to check how the system behavior changes with the dimensionless parameter $\xi = g/(f_s a^4)$ ($\xi \sim 1$ corresponds to a very strong interaction). Summing up, all parameters can be very reasonably estimated for a given experimental system.

For our exemplification, we concentrate now specifically on the recent very detailed SFB boundary lubrication experiment due to Klein [4]. The top and bottom surfaces are in contact over an area A across a thin OMCTS film of thickness $h = 3.5 \pm 0.3\,\text{nm}$ (four molecular layers), under a load $F_l = 42\,\mu\text{N}$. The slider total mass $M \approx 1.47\,\text{g}$ is subject to a lateral force via a spring of constant $K = 97\,\text{N m}^{-1}$ pulled with velocity $v_d = X_0/\tau_0 \sim 10^{-2}\,\mu\text{m s}^{-1}$ ($X_0 \approx 80\,\text{nm}$, $\tau_0 \approx 8\,\text{s}$). Slip begins as the yield stress KX_0/A is reached. The top surface slips past the bottom surface for a time $\tau_s \approx 0.025\,\text{s}$ by an amount $\Delta X_0 \sim 60\,\text{nm}$, when the slider sticks; and so on. The time per stick-slip cycle is $\tau_{ss} \approx 1\,\text{s}$. In the experiment [4], the slip curve $X(t)$ is fit by a homogeneous equation $M\ddot{X} + B\dot{X} = K(X_d - X)$, where $B = A\tilde{\eta}/h$, assuming that the shear-melted film behaves as a Newtonian liquid with zero-fluid-velocity boundary conditions, and effective viscosity $\tilde{\eta}$ independent of the shear rate. The fit yields $\tilde{\eta} = 27 \pm 4\,\text{Pa s}$, exceeding by a factor of 10^4 the bulk viscosity of OMCTS ($\tilde{\eta}_{\text{bulk}} = 2.5 \times 10^{-3}\,\text{Pa s}$). At the instant of stick, when the film is assumed to solidify, the slider undergoes ''ringing'' vibrations (decaying oscillations) with a frequency $\nu_c \approx 45\,\text{Hz}$ (notice that $\Omega_S = (K/M)^{1/2} = 257\,\text{s}^{-1}$, or $\nu_S = \Omega_S/2\pi = 41\,\text{Hz}$). The static friction threshold is $F_s = 18\,\mu\text{N}$ [4,22,23], and for the area one may take values given by Klein and Kumacheva [22,23], $A \approx 10^{-10}\,\text{m}^2$.

Table 1. Simulation parameters.

Parameter	Value	Comment
M	1.47×10^{-3} kg	Ref. [4]
K	$97\,\mathrm{N\,m^{-1}}$	Ref. [4]
h	3.5×10^{-9} m	Ref. [4]
A	$10^{-10}\,\mathrm{m^2}$	Ref. [22,23]
F_s	18 μN	Ref. [4,22,23]
Ω_S	$257\,\mathrm{s^{-1}}$	Ref. [4]
η_S	$51.4\,\mathrm{s^{-1}}$	$0.2\ \Omega_S$
N	4080	
f_s	4.41×10^{-9} N	F_s/N
m	8.2×10^{-20} kg	$(A/N)\ h\rho_{\mathrm{OMCTS}}$
k	$0.49\,\mathrm{N\,m^{-1}}$	$Nk \gg K$
η	$2 \times 10^{11}\,\mathrm{s^{-1}}$	bulk value
τ_d	5×10^{-4} s	
v_d	$0.1\,\mu\mathrm{m\,s^{-1}}$	

To summarize, our simulations explored the following parameters (see Table 1): $M = 1.47$ g, $K = 97\,\mathrm{N\,m^{-1}}$, $h = 3.5 \times 10^{-9}$ m, $A = 10^{-10}\,\mathrm{m^2}$, $F_s = 18$ μN, and $f_s = F_s/N$. The contact area $A_i = A/N$ defines the contact mass $m = A_i h \rho_{\mathrm{OMCTS}}$, and the lubricant damping coefficient is $\eta = 2 \times 10^{11}\,\mathrm{s^{-1}}$ assuming the *ordinary* bulk viscosity $\tilde{\eta}_{\mathrm{OMCTS}}$. Then $m_i = m\ f_{si}/f_s$, $k_i = k(f_{si}/f_s)^{1/2}$ (see Appendix A in Ref. [17]), and we assume that $\eta_i = \eta$. The damping inside the slider can be found from the experimentally observed decay of ringing oscillations, yielding $\eta_S = 0.2\,\Omega_S$. Finally, the driving velocity value in simulation $v_d = 0.1\,\mu\mathrm{m\ s^{-1}}$ is as usual taken larger than in experiment so as to yield a viable simulation time, without any essential differences or problems.

For other model parameters, not directly extractable from experiment, we used $N = 4080$ for the number of contacts, $f_b = 0.1 f_s$ for the backward force, $\Delta f_s = 0.01 f_s$ for the threshold dispersion, and $\tau_d = 5 \times 10^{-4}$ s for the delay time. As for the elasticity of the contacts, an estimation from $k \approx \rho c^2 a_i$ yields $kN \sim 10^2 \sqrt{N}\,\mathrm{N\,m^{-1}}$. In simulations, we used $kN = 2000\,\mathrm{N\,m^{-1}}$ so that the condition $Nk \gg K$ is satisfied (note that excessive k values would yield Runge–Kutta steps too small to be handled). For these few relatively arbitrary parameters, we took care to check systematically the stability of physical results against reasonable variations.

4. Simulated kinetics

A typical example of stick-slip motion and frictional force resulting by simulation of our EQ model with the chosen parameters is presented in Figure 2. As one can see by comparing with Figures 1 and 2 in Ref. [4], the theoretical stick-slip is quite similar to the experimental data, including the large initial stick spike and subsequent spikes of smaller amplitude. In the following, we address the underlying physics of this overall result for the spring force $F(t) = K[v_d t - X(t)]$, with its detailed aspects and their dependence upon model parameters.

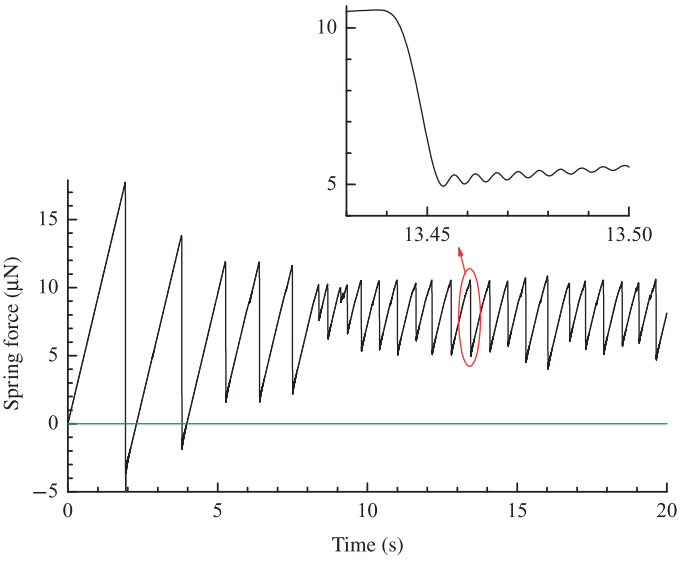

Figure 2. Calculated slider spring force in the stick-slip regime. Parameters as given in the text, and $\xi = 0$. The inset shows the detail of a slip, with the sudden force drop and mechanical ringing oscillations.

4.1. *Elastic instability*

Stick-slip generally appears as the result of an elastic instability of the pinned state [1,18]. Firstly let us consider the case of a rigid slider, $K = \infty$. This case was studied in [16,17], where the evolution law of the system reduced to a master equation, allowing an analytical investigation. When the slider begins to move adiabatically, $\dot{X} > 0$, it experiences a friction force $F_\infty(X) < 0$ from the interface. At the beginning $|F_\infty(X)|$ grows linearly with X, $|F_\infty(X)| \approx NkX$, until it reaches a value $\sim F_s - \Delta F_s$. Here many contacts have broken and are not yet reformed, and the growth gives way to a drop during a displacement $x_* \sim \Delta f_s/k$ down to $F_b = Nf_b$. At this point a majority of contacts (though no longer all of them) have been reborn, and sliding hardens again.

The same picture remains qualitatively correct if the slider is not rigid but stiff enough, $K > K^*$, where

$$K^* = \max F'_\infty(X), \quad F'_\infty(X) \equiv \frac{\mathrm{d}F_\infty(X)}{\mathrm{d}X},$$

provided the driving velocity is not too high so that the motion is adiabatic (a condition easily satisfied in experiment). The time dependent spring force $F(t)$ is, according to Newton's third law, to be compensated by the force from the interface, $F(t) + F_\infty[X(t)] = 0$. If the slider is soft enough, $K < K^*$, the slider motion becomes unstable at the point X_c, where X_c is the (lowest) solution of the equation $F'_\infty(X) = K$. Let this occur at the instant t_c. After the unstable point, $t > t_c$, the equation of motion for $\Delta X = X - X_c$ and $\Delta t = t - t_c$ is

$$M\Delta\ddot{X} + M\eta_S\left(\Delta\dot{X} - \langle\Delta\dot{X}\rangle\right) = F_\infty(X_c + \Delta X) - F_\infty(X_c) + Kv_d\Delta t - K\Delta X, \qquad (4)$$

which has to be solved with the initial condition $\Delta X = 0$ and $\Delta\dot{X} = v_d$ at $\Delta t = 0$.

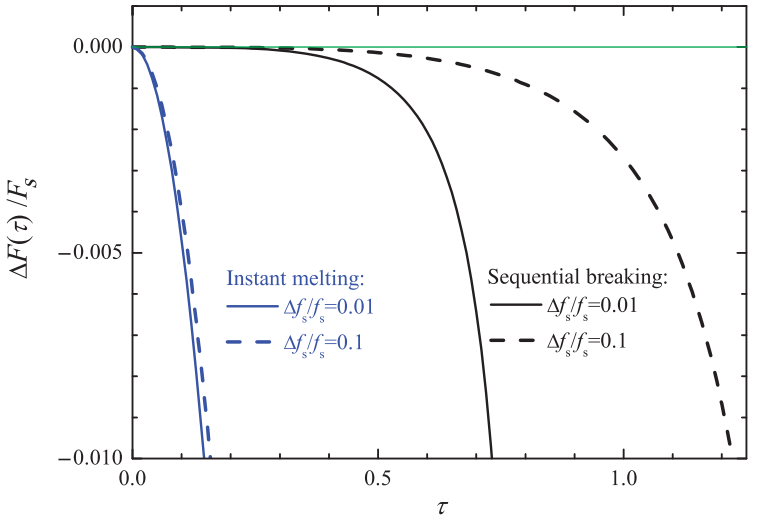

Figure 3. Drop of the spring force $\Delta F(\tau)/F_s = D_1\tau - x(\tau)$ versus dimensionless time $\tau = \Omega_S(t - t_c)$ for the slider motion after the unstable point ($X > X_c$) according to numerical solution of Equation (5) (right-hand, black curves, sequential breaking of contacts) or Equation (6) (left-hand, blue curves (color online), instant melting of the lubricant) for $\Delta f_s/f_s = 0.01$ (solid curves; $D_0 = 0.94$, $D_1 = 2.1 \times 10^{-3}$, $D_2 = 2.2 \times 10^5$, $D_3 = 1.91$; $\eta = \eta_S = 0$) and for $\Delta f_s/f_s = 0.1$ (dashed curves; $D_0 = 0.794$, $D_2 = 3.61 \times 10^3$, $D_3 = 4.03 \times 10^{-2}$).

In our model, the function $F_\infty(X)$ near the point X_c can be approximated as $F_\infty(X) \approx F_\infty(X_c) + F'_\infty(X_c)\,\Delta X + \frac{1}{2}F''_\infty(X_c)\,\Delta X^2 + \frac{1}{6}F'''_\infty(X_c)\,\Delta X^3$, so that $F_\infty(X_c + \Delta X) - F_\infty(X_c) - K\Delta X = \frac{1}{2}F''_\infty(X_c)\,\Delta X^2 + \frac{1}{6}F'''_\infty(X_c)\,\Delta X^3$. Introducing the dimensionless variables $x = K(X - X_c)/F_s$ and $\tau = \Omega_S(t - t_c)$, we obtain for the slider coordinate

$$\frac{\mathrm{d}^2x(\tau)}{\mathrm{d}\tau^2} + \frac{\eta_S}{\Omega_S}\left(\frac{\mathrm{d}x(\tau)}{\mathrm{d}\tau} - \left\langle\frac{\mathrm{d}x(\tau)}{\mathrm{d}\tau}\right\rangle\right) = D_1\tau + D_2x^2 + D_3x^3, \tag{5}$$

where $D_1 = v_d\sqrt{KM}/F_s$, $D_2 = \frac{1}{2}[F''_\infty(X_c)/F_s](F_s/K)^2$, and $D_3 = \frac{1}{6}[F'''_\infty(X_c)/F_s](F_s/K)^3$. Solution of Equation (5) should be sought with the initial condition $x(0) = 0$ and $\mathrm{d}x(\tau)/\mathrm{d}\tau|_{\tau=0} = D_1$. At short times, $\tau \ll 1$, the solution has the form $x(\tau) \approx D_1\tau + \frac{1}{6}D_1\tau^3$. Thus, as $X(t)$ grows at $t > t_c$, the spring force decreases during a slip time – determined by the setup inertia – $\tau_s \approx \alpha\Omega_S^{-1}$ in the form

$$F(t) \approx F(X_c) - (K^2v_d/6M)(t - t_c)^3,$$

where $\alpha = (6\ F_s\Omega_S/K\ v_d)^{1/3}$ ($\alpha \approx 2.21$ for the chosen set of parameters). Numerical solution of Equation (5) is shown in Figure 3 (right-hand curves).

If, by contrast, the lubricant film were hypothetically to melt instantly and as a whole at $t = t_c$, then for $t > t_c$ we would have $F_\infty(X_c + \Delta X) = -M\eta\,\Delta\dot{X}$, and the motion would be described by

$$\frac{\mathrm{d}^2x(\tau)}{\mathrm{d}\tau^2} + \frac{\eta}{\Omega_S}\frac{\mathrm{d}x(\tau)}{\mathrm{d}\tau} + \frac{\eta_S}{\Omega_S}\left(\frac{\mathrm{d}x(\tau)}{\mathrm{d}\tau} - \left\langle\frac{\mathrm{d}x(\tau)}{\mathrm{d}\tau}\right\rangle\right) = D_1\tau + D_0 - x, \tag{6}$$

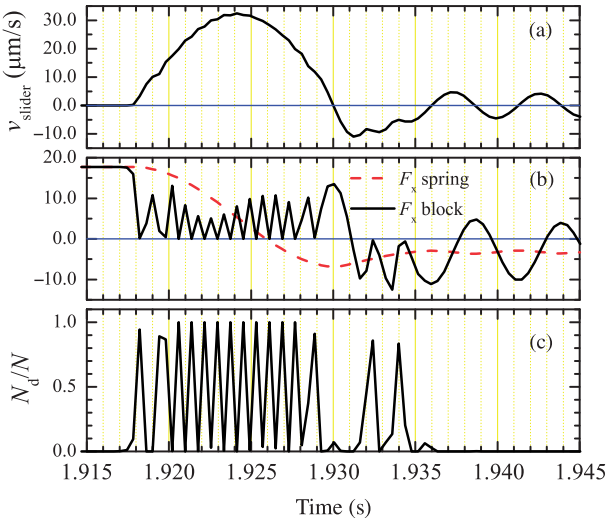

Figure 4. Details of the first large slip shown in Figure 2: (a) the slider velocity; (b) the spring force F (dashed curve: red online) and the force from contacts F_B (solid curve); and (c) the number of detached contacts N_d as functions of time.

where $D_0 = F_\infty(X_c)/F_s$. In this case, the solution for $\tau \ll 1$ is $x(\tau) \approx D_1\,\tau + B\tau^2$, so that the spring force drop at slip is given by

$$\Delta F(\tau)/F_s \approx -B\tau^2$$

with $B = \frac{1}{2}(D_0 - \eta D_1/\Omega_S)$. This gives a slip time $\tau_s \approx \beta\Omega_S^{-1}$ with $\beta = [2/(D_0 - \eta D_1/\Omega_S)]^{1/2}$. Numerical solution of Equation (6) is shown in Figure 3 (left-hand curves). An estimation gives $\beta \approx [2/(1-b)]^{1/2}$ with $b = \eta m v_d/f_s \approx 3.7 \times 10^{-7}$ for the chosen set of parameters. The main outcome is that by assuming instant overall lubricant melting the resulting slip time is shorter than in the multi-contact case. Of course one may make τ_s as large as desired by using artificial values for the lubricant viscosity η orders of magnitude larger than the bulk value; but except for a monatomic film, there are, as was said, no physical grounds for that assumption.

4.2. *Slip details*

Details of the slip such as the slider velocity, the force exerted by the contacts, and the number of broken contacts are shown in Figure 4. During the slip time τ_s, the slider velocity grows up to a value $v_m \sim \Omega_S\, F_s/K$. As the slider accelerates, contacts break, and the force $F_B(t)$ acting on the slider from the contacts drops and rises with increasing frequency between zero and a maximum value, the latter less and less able to compensate the spring force $F(t)$ (dashed in Figure 4). This continues until after a typical reforming time similar to τ_d (here of order 5 msec) enough contacts are reborn so that the acceleration reverses. From this point the peak values of $F_B(t)$ after each breaking grow as $F_B(t) = Ct$ with a rate $C = Nkvt$ eventually becoming

large enough to cross the slowly decreasing spring force $F(t)$ (in Figure 4 that crossing is reached around $t = 1.924$ s). Here the spring and the block reaction forces compensate, and the sliding undergoes arrest. In fact the slider even retracts slightly, as it first settles by breaking a few contacts backwards, and then oscillates about its newly reached stuck state. Therefore, during an individual slip the substrate reaction force F_B oscillates with a rough period $\tau_B \approx F_s/Nkv_m \approx K/Nk\Omega_S$ between successive contact breakings. This contact-breaking feature should form a strong observable component of time-dependent frictional noise, always present provided that $\tau_B < \tau_s$, or $K < Nk$. By contrast, no such multi-contact noise is expected for uniform lubricant melting; future experiments might in principle distinguish the two mechanisms just based on that.

4.3. *Ringing*

Following the slip, the slider sticks, and the spring force shows ringing. For $\tau_d < \Omega_S^{-1}$, ringing occurs with a high frequency $\Omega_L = (Nk/M)^{1/2} = 1.17 \times 10^3\,\mathrm{s}^{-1}$ (so that $\tau_L \equiv 2\pi/\Omega_L = 5.39 \times 10^{-3}$ s). During the slip, many contacts reform so that the spring force drops to values that are positive and much higher than F_b [10].

The ringing frequency slows down when $\tau_d > \Omega_S^{-1}$. In this case, the spring force drops to negative values and then oscillates around zero with the frequency Ω_S during the time τ_d. The contacts reform well after the slip has occurred, leading to a stable stick-slip steady state.

The ringing vibration amplitude decays as $e^{-\eta_S t}$ because of the internal damping introduced in Equations (2) and (3). When that is neglected, the dependence F versus $v_d t$ takes a ''universal'' form (compare Figures 2 and 5). Thus, if the velocity is so small that $\tau_{ss} \gg \eta_S^{-1}$ and the ringing oscillations are completely damped during the time τ_{ss} before the next slip, then the details of ringing do not influence the stick-slip. If on the contrary the driving velocity is so high that $\tau_{ss} \lesssim \eta_S^{-1}$, then the oscillations disturb the system dynamics and may even eventually lead to smooth sliding.

4.4. *Dependence upon model parameters*

The steady state behavior of the slider, either stick-slip or smooth sliding, is controlled by two model parameters – the contact reforming time τ_d and the dispersion Δf_s of micro-contact breaking thresholds. Indeed, one may suppose that the elastic instability will always result in stick-slip motion. However, the condition $K < K^*$ is only necessary but not sufficient for stick-slip; the second condition is to have a nonzero delay time, $\tau_d > 0$. This was demonstrated in our previous work [10]: if $\tau_d = 0$, despite some initial stick-slips, the system eventually approaches smooth sliding. We note that in Persson's original simulation [13] of the EQ model, where stick-slip was demonstrated, the delay time τ_d corresponded to the contact sliding time necessary for its velocity to fall to zero. The same is demonstrated below in Section 6, where we present results of MD simulation for the system. However, the sliding time is only one (relatively small) contribution to τ_d.

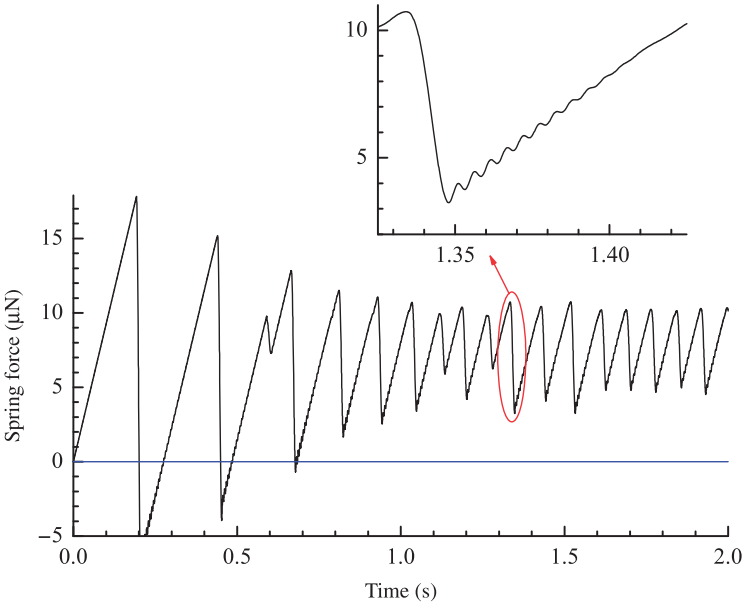

Figure 5. Frictional spring force calculated with the same parameters as in Figure 2 but with a higher driving velocity $v_d = 1\,\mu\text{m s}^{-1}$.

Then, the existence of the elastic instability itself is controlled by the dispersion Δf_s of micro-contact breaking thresholds. In fact

$$K^* = \max F'_\infty(X) \approx Nkf_s/\Delta f_s. \tag{7}$$

Thus, if Δf_s is small enough to cause $K^* > K$, then we have stick-slip; otherwise there is smooth sliding. In the stick-slip regime, an increase of Δf_s leads to the decrease of the stick-slip period τ_{ss} (see [10]). The slip time τ_s characterizing the drop of spring force $F(t)$ during slips also increases with Δf_s, although only slightly, because the distribution of threshold displacements $x_{si} = f_{si}/k_i$ rather than the distribution of the threshold forces f_{si} plays the main role in system kinetics. The distribution of x_{si} is narrower than the distribution of f_{si}, because f_{si} and k_i tend to change synchronically due to the relationship $k_i \propto f_{si}^{1/2}$. The ratio $\Delta f_s/f_s$ should typically decrease with the time of stationary contact due to aging of contacts during stick. This agrees with earlier arguments that aging is responsible for the much lower velocity of the transition from stick-slip to smooth sliding observed in experiment when compared to MD simulations [1,2,16,17,21].

The precise values of other parameters of the model are inessential. For example, Figures 6 and 7 demonstrate the change of system behavior for different values of the parameters f_b and k, respectively. Moreover, the slip time remains approximately unchanged even if we increase the model parameter η (which corresponds to the film "viscosity" in the uniform melting interpretation of boundary layer stick-slip) by a factor 10^5 as demonstrated in Figure 8.

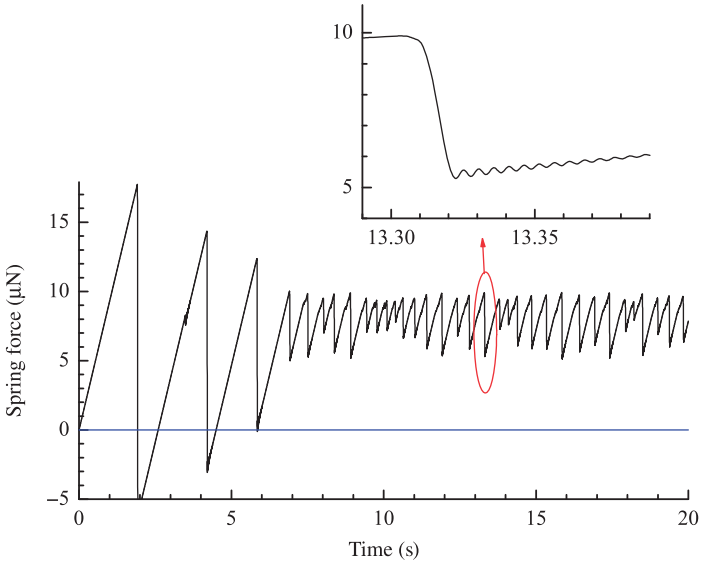

Figure 6. The same as in Figure 2 but for a lower backward force $f_b = 0.01\, f_s$.

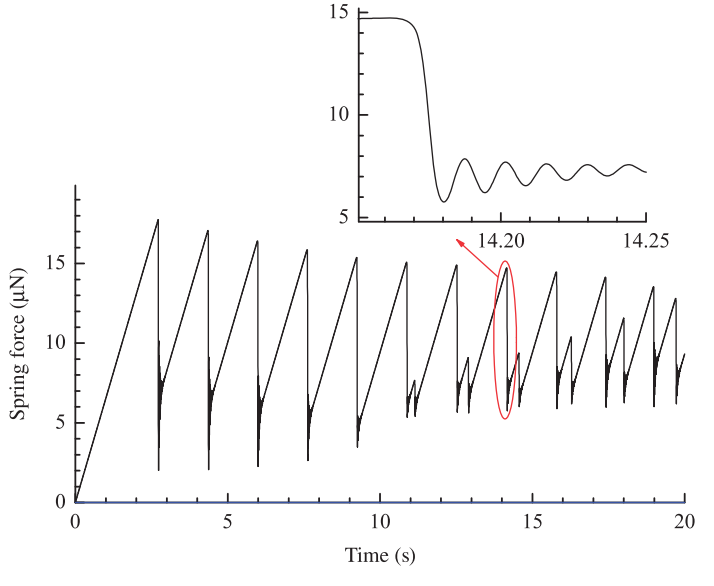

Figure 7. The same as in Figure 2 but for softer contacts with $kN = 200\,\mathrm{N\,m^{-1}}$.

5. Interaction between contacts

Special attention must be devoted to study the role of interactions between the contacts, introduced in Section 2. Roughly speaking, the interaction influences the system kinetics in the same way as a narrowing the dispersion Δf_s: the stronger the interaction, the wider the range of model parameters where stick-slip operates.

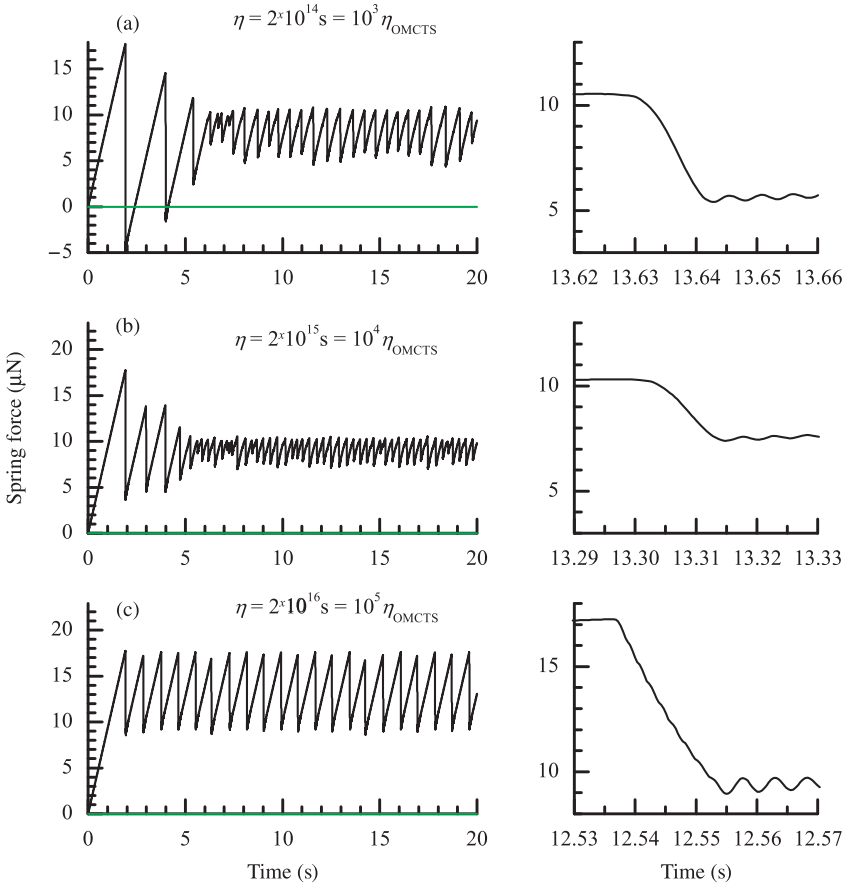

Figure 8. Dependences $F(t)$ for different lubricant viscosity η (other parameters as in Figure 2).

To demonstrate this result, we calculated with the help of the EQ algorithm the system kinetics with increasing interaction ($\xi = 0$–0.3) using softer contacts ($kN = 200\,\mathrm{N/m}$) and larger dispersion $\Delta f_s/f_s = 0.3$. The results are presented in Figure 9. For this choice of parameter, the system quickly goes to smooth sliding in the case of zero interaction (Figure 9a), but develops stick-slip for strong interaction $\xi = 0.3$ (Figure 9d). Details of the slip are shown in Figure 10: without interaction, the detaching of contacts is sequential (Figure 10a), while for a strong interaction, all contacts tend to detach simultaneously, and the force F_B drops much more abruptly to zero (Figure 10d). The interaction may lead to the appearance of an avalanche of contact breaking as was described in [3]. Whereas for $\xi = 0$ the contacts break sequentially, one after the other, for $\xi > 0$ one contact breaking may trigger the breaking of the nearest contacts, and generate an avalanche whose average size increases with ξ as shown in Figure 11. For large enough strength of interaction, here $\xi = 0.3$, the avalanche may cover the whole system (Figure 11d).

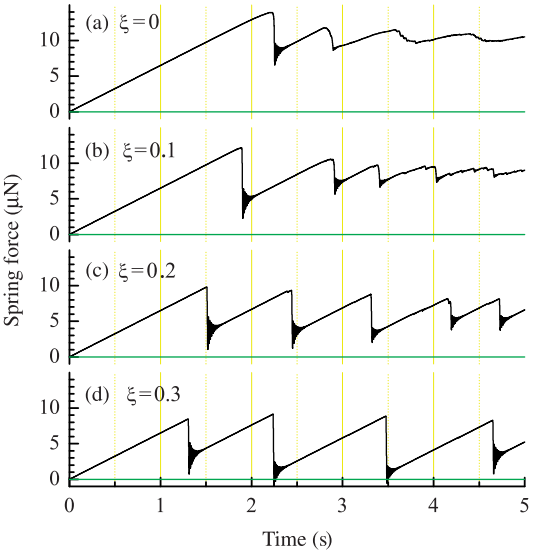

Figure 9. Dependence of the frictional spring force $F(t)$ for different strengths of the contact–contact interaction ξ from no interaction (a) to a strong interaction (d). $kN = 200\,\mathrm{N\,m^{-1}}$, $\Delta f_s/f_s = 0.3$.

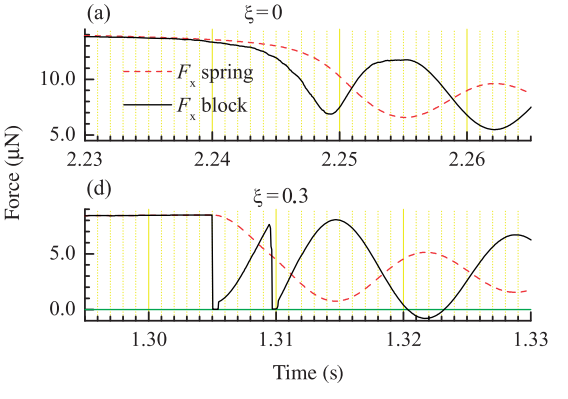

Figure 10. Frictional spring force $F(t)$ (dashed: red online) and block interface force F_B (t) (black solid curve) during slip for (a) noninteracting and (d) strongly interacting contacts. Parameters as in Figure 9.

Analytical expressions for the avalanche size have been given in [3]. If we write the force due to interaction between the contacts 1 and 2 as $f_{\mathrm{int}} = k_{\mathrm{eff}}(x_1 - x_2)$, then $k_{\mathrm{eff}} = 3\,\xi f_s/a = 3\,\xi F_s/\sqrt{AN}$. The interaction becomes important if $k \sim \nu k_{\mathrm{eff}}$, where $\nu \approx 4$ is the number of nearest neighbors. Defining ξ^* by the equation $k = \nu k_{\mathrm{eff}}$, we expect that the interaction is irrelevant if $\xi \ll \xi^*$, while in the opposite case the interaction is so strong that all contacts move together. For the chosen set of model

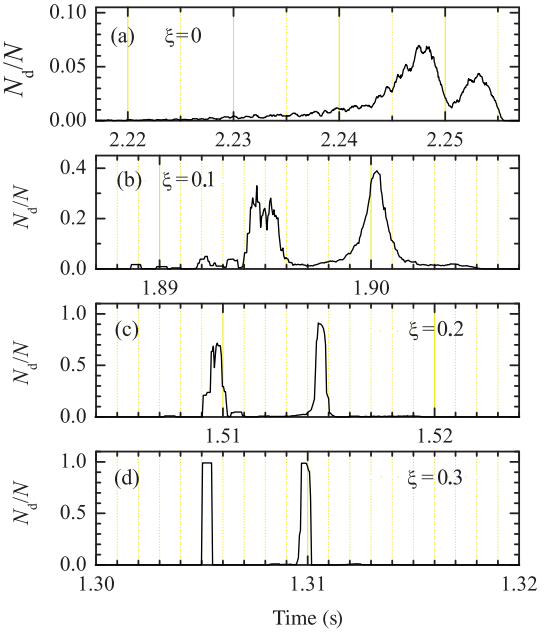

Figure 11. Time dependence of the number of broken contacts $N_d(t)$ during slip for different interaction strengths. Parameters as in Figure 9.

parameters and $kN = 200\,\mathrm{N\,m^{-1}}$ we obtain $\xi^* \approx 0.15$ in agreement of the numerical results of Figure 11.

6. MD simulation including contact interactions

The cellular automata EQ algorithm used above completely ignores real dynamics of the contacts. To remedy that, we apply the molecular dynamics approach. While of course MD is much more realistic, it has a problem of time-scales. The individual motions of the contacts are characterized by a frequency $\omega_l = (k/m)^{1/2} = 7.73 \times 10^8\,\mathrm{s^{-1}}$, whose inverse sets the time step size. The bottleneck is the slow characteristic slip time, equal to the inverse inertial slider frequency $\Omega_S = (K/M)^{1/2} = 2.57 \times 10^2\ \mathrm{s^{-1}}$. This is many orders of magnitude longer, hard to manage in a brute force MD simulation. The problem may be circumvented with the help of a trick. If we reduce artificially the slider mass, say $M \to \tilde{M} = s^3 M$ with a scaling factor $s \ll 1$, this will increase the characteristic slider frequency, $\tilde{\Omega}_S = (K/\tilde{M})^{1/2} = s^{-3/2}\Omega_S$. If at the same time we rescale other dynamical variables in the form $F_s \to \tilde{F}_s = s^2 F_s$, $t \to \tilde{t} = s^{3/2} t$, $X \to \tilde{X} = s^2 X$, and $v \to \tilde{v} = s^{1/2} v$, then the dependence $F(t)$ remains almost unchanged, so long as the rescaling leaves the motion of individual contacts still much faster than that of the whole slider. The virtual independence of the frictional force upon s is demonstrated in Figure 12.

Comparison of the simulation results obtained with the EQ algorithm with those of the MD simulation presented in Figures 13 and 14 demonstrates two

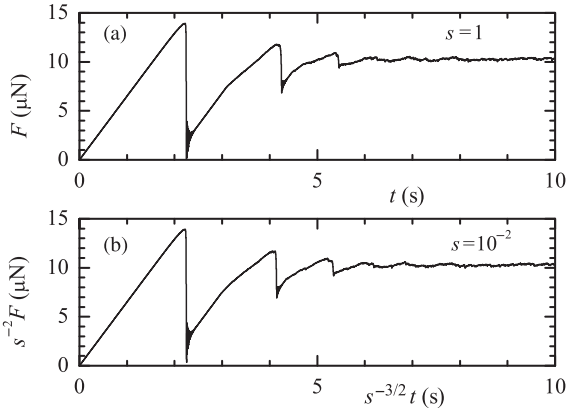

Figure 12. Spring force versus time for the EQ algorithm for two values of the scaling factor $s=1$ (a) and $s=10^{-2}$ (b). $\Delta f_s/f_s=0.3$, $kN=200\,\mathrm{N\,m^{-1}}$, $\tau_d=0.005$ s; other parameters as in Figure 2.

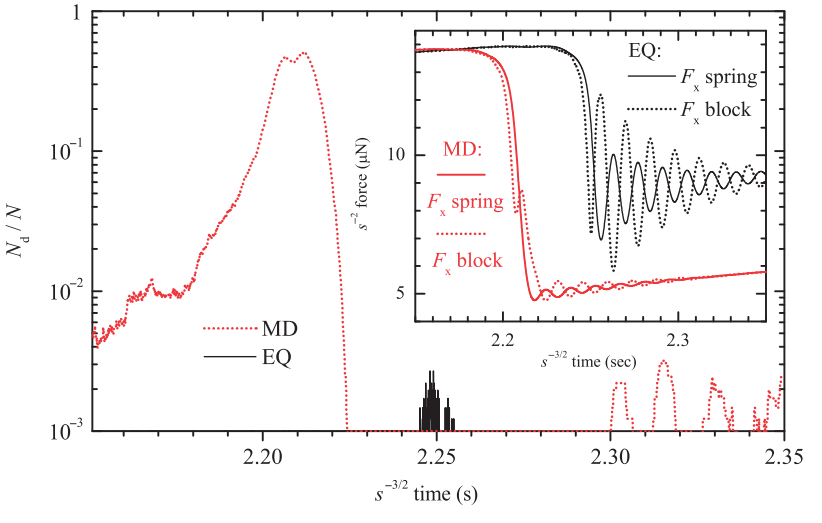

Figure 13. Slip dynamics of the EQ and MD algorithms with the scaling factor $s=10^{-2}$. The number of detached contacts versus time for EQ (black solid) and MD (short-dotted: red online). Inset: the spring force (solid) and the force from contacts (short-dotted) for EQ (right-hand, black curves) and MD (left-hand, red curves: color online). $\Delta f_s/f_s=0.3$, $kN=200\,\mathrm{N\,m^{-1}}$, $\tau_d=0$; other parameters as in Figure 2.

important features. Firstly, in the EQ algorithm the contact sliding time τ_c is zero, while $\tau_c>0$ for real MD dynamics. According to Figure 13, the number of detached contacts is nonzero for a time interval of the order of $\tilde{\tau}_c\sim 0.1$, or, in unrescaled units, during a time of $\tau_c=s^{3/2}\tilde{\tau}_c\sim 10^{-4}$ s, which is much longer than that predicted by the crude estimate given above in Section 2. Thus, in a real system the delay time

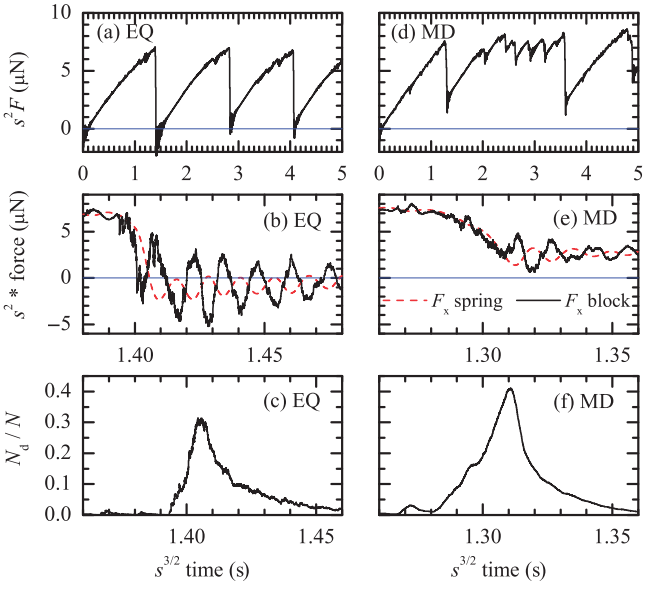

Figure 14. Dynamics of the model calculated with the EQ (a)–(c) and MD (d)–(f) algorithms for the interacting contacts with $\xi = 0.04/s^2$. The top panels (a), (d) show several stick-slip cycles, while the middle and bottom panels show details of one slip, the spring ($F(t)$, dashed: red online) and interface (F_B (t), solid curve) forces (b), (d) and the number of detached contacts (c), (f) as functions of time. The parameters are as in Figure 13.

$\tau_i = \tau_c + \tau_f$ is always nonzero, even if the contact reforming time τ_f is zero. Therefore, a real system should always exhibit stick-slip behavior provided $K < K^*$, although the amplitude of stick-slip may be very small and masked by ringing.

Secondly, the EQ and MD simulated avalanche dynamics for the system of interacting contacts ($\xi > 0$) are also different: an avalanche propagates instantly with the EQ algorithm, while in the MD case, it does that at a finite rate as demonstrated in Figure 14. In this respect, the MD result is more accurate, whereas the instantaneous propagation in EQ appears to be a mean-field artifact. An investigation of the concerted motion of contacts, e.g. calculation of the size, shape and evolution of the avalanche of broken contacts, deserves a separate study which lies outside the scope of the present work.

7. Nonrigid sliders

In our schematic model of the SFA/SFB setup shown in Figure 1, the sliding mass M is concentrated at the end of the driving spring, i.e. the slider plus spring form a pendulum. In a more realistic situation, however, we must forgo rigidity of the slider; both its mass and elasticity are distributed through the slider as shown in Figure 15. One may think that in this case, only the lowermost slider atomic layer starts to move at the onset of slip. Therefore, a characteristic frequency will be defined by the mass M_l of the layer and its rigidity K_l, which will lead to a much higher

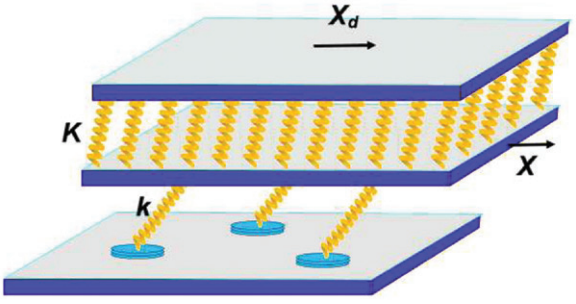

Figure 15. The earthquake-like model with a nonrigid slider.

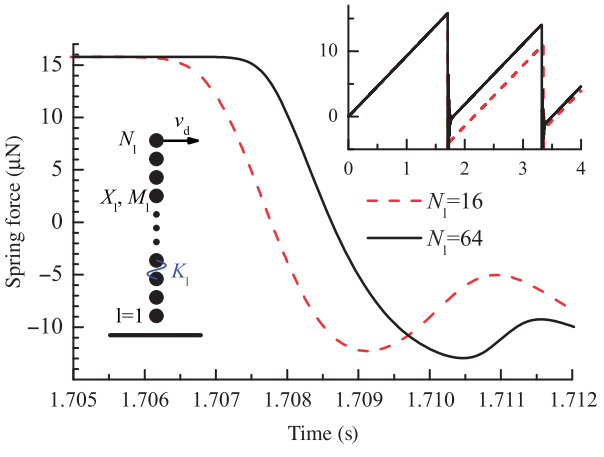

Figure 16. Slip kinetics for the nonrigid slider consisting of $N_l = 16$ (dashed: red online) or $N_l = 64$ (black solid curve) layers (top-right inset shows the whole stick-slip cycle). Bottom-left inset shows the layered model of the slider: the first layer is in contact with the bottom substrate, while the last layer is moved with the velocity v_d.

(atomic scale) frequency. A similar question – which mass, either the total mass M or the layer mass M_l, defines the time-scale of the system – already appeared in the problem of minimal velocity for atomic-scale smooth sliding. As was proven elsewhere [21], if the slider velocity decreases, first the lowermost layer stops; then a so-called stopping wave emerges and removes the kinetic energy of the rest of the slider. As a result, the time-scale of the problem is determined by the layer mass M_l, and the minimal velocity is of atomic-scale order of $\mathrm{m\,s^{-1}}$. Now, however, the situation is just the opposite – the time-scale of the onset of sliding is determined by the total slider mass M and its rigidity K.

To show this, let us consider a model similar to that used in [21]. Let the slider consist of N_l layers, each of mass $M_l = M/N_l$, elastically coupled by springs of elastic constant $K_l = K\ N_l$ (see the inset in Figure 16). In the stationary state, when the

bottom layer is fixed and a force F is applied to the top layer, the latter will shift on the displacement $\Delta X = \sum_{l=1}^{N_l} \Delta X_l$, where $\Delta X_l = F/K_l$, so that $\Delta X = F/K$ as before in the rigid-slider model. Now let the top layer be driven with the velocity v_d, while the bottom layer be in contact with the bottom substrate as before. The dependence of the elastic force within the slider on time, obtained with simulation for two different values of N_l, is presented in Figure 16 (note that now we may discard the artificial damping η_S in the equations of motion, because internal degrees of freedom are included). As seen, the slip kinetics is almost independent of the number of layers N_l and is determined by the minimal slider mechanical frequency Ω_S.

The frequency Ω_S can be found with the help of elasticity theory [24]. Let the slider have a cylindrical shape of height L and radius r, and be characterized by the section $S = \pi r^2$, geometrical inertial momentum $I = \frac{1}{4}\pi r^4$, mass density ρ and Young's modulus E. If the cylinder foot is fixed and a force F is applied to its top, the latter will be shifted by a distance $\Delta X = FL^3/3EI$ (the problem of a bending pivot, see [24], Section 20, example 3). Thus, the effective elastic constant of the slider is $K = 3EI/L^3$. The minimal frequency of bending vibration of the pivot with one fixed end and one free end is given by $\Omega_S = (3.52/L^2)\ (EI/\rho S)^{1/2}$ (see [24], Section 25, example 6). Taking $M = \rho SL$, we obtain $\Omega_S \approx 2.03\ (K/M)^{1/2}$.

The frequency of ringing vibrations after the slip is either Ω_S (if $F(t)$ oscillates around zero in the case of $\tau_d > \Omega_s^{-1}$) or Ω_L, i.e. much higher in the case of $\tau_d < \Omega_s^{-1}$. However, the question is more involved: in the model we assumed that the bottom substrate (the base) is rigid and fixed. In a real setup, only the bottom of the base is fixed, while the base has its own mass M_B and elasticity K_B. When the sliding stops and the two substrates are pinned together, the whole system of mass $M_\Sigma = M_B + M + Nm$ should oscillate with a frequency $\sim (K_B/M_\Sigma)^{1/2}$. Unfortunately, we do not know the experimental value for the parameter K_B.

The elastic energy stored in the interface and the substrates during stick is dissipated during slip as well as during subsequent ringing oscillations. The latter can easily be estimated if the amplitude and frequency of these vibrations are known. The other part of the stored energy is dissipated during slip when $F(t)$ drops. Every contact's sliding-stopping event excites phonons in the substrates, and the energy is dissipated continuously at every breaking-reforming of individual contacts before it finally goes to substrate heating.

8. Discussion and comparison with experimental SFB boundary friction

We can now compare our results with the boundary lubrication data provided by Ref. [4], where SFB measurements between mica surfaces with a four-layer OMCTS lubricant film were carried out as described in Section 3. The interpretation originally provided to account quantitatively for the slow observed slip time was that the lubricant melted as a whole at slip, and that the viscosity of the confined fluid could be as high as 10^4 times that of bulk OMCTS.

The mechanism of slip onset (either sequential breaking of the contacts or the instant melting of the lubricant film) determines the details of the slip kinetics which in principle may be resolved with precise SFA/SFB experiments. Firstly, the initial decrease of the spring force at the onset of slip should follow the law $\Delta F(t) \propto (t - t_c)^3$

for the EQ model, while instantaneous melting will exhibit the dependence $\Delta F(t) \propto (t - t_c)^2$ (see Figure 3). Moreover, in the instantaneously-melting case the sliding starts (i.e. the slider velocity begins to increase) when $F'(t_c) \geq 0$, while for the EQ mechanism, $F'(t_c) < 0$. Secondly, during slips the substrate reaction force F_B should oscillate with the period $\tau_B \approx K/Nk\Omega_S$ as described above in Section 4.2. This contact-breaking feature may form an observable component of time-dependent frictional noise, always present provided $K < Nk$, while no such multi-contact noise is expected for uniform lubricant melting.

The order of magnitude of the slip time τ_s during which $F(t)$ drops is in both cases determined by the inverse mechanical frequency $\Omega_S^{-1} = (K/M)^{-1/2}$ of the setup. In our multi-contact model, this time remains approximately unchanged even if we increase the model parameter η (which corresponds to the film "viscosity" in the uniform melting interpretation of boundary layer stick-slip) by a factor of 10^5 as shown in Figure 8. This point might easily be checked experimentally by changing, for example, the loading force, because the force damping associated with the lubricant viscosity in the uniform melting interpretation is directly proportional to the contact area, which in turn is roughly proportional to the load. The large viscosity of the thin confined lubricant film inferred in the uniform melting model is therefore strongly questioned by our model, where the same data are explained by realistic inhomogeneous multi-contact sliding. In our model, the drop of the spring force $F(t)$ is gradual not because viscosity is high, but as a consequence of the slowing down and consequent breaking (melting) of different contacts (domains).

9. Conclusions

In summary, given the problem of mesoscopic boundary lubrication, we have

(i) described the slip dynamics in detail in the presence of multi-contact inhomogeneity;
(ii) considered the effect of elastic interactions between the contacts;
(iii) considered the real dynamics of sliding contacts with the help of molecular dynamics, highlighting the difference between that and predictions of the EQ algorithm;
(iv) considered the effects of elasticity of the sliders.

Our main conclusion is that a realistic model of dry friction or boundary lubrication of mesoscopic or macroscopic size sliders must first of all incorporate the distribution of static thresholds. The stick-slip motion takes place if and only if two conditions are satisfied: first, the slider is soft, $K < K^*$, where K^* is defined by the interface properties, Equation (7), and second, the delay time for contact reforming is nonzero, $\tau_i \geq \tau_d > 0$. If at least one of these conditions is violated, the steady-state motion reduces to smooth sliding, and stick-slip is lost. However, the MD simulation, where atomistic motion of contacts is directly incorporated, shows that the latter condition, $\tau_i > 0$, should be satisfied "automatically".

Our second result concerns the investigation of the role of elastic interaction between the contacts. We showed that this interaction leads to "effective narrowing" of the distribution of static thresholds. Therefore, even if the dispersion of thresholds

is rather large, e.g. $\Delta f_s/f_s \sim 1$ as in the case of contact of rough surfaces [17], the stick-slip motion may nevertheless be realized due to concerted sliding of the contacts.

Thirdly, we discussed the problem of the effective viscosity of a thin lubricant film. The tribological setup may be treated as a damped pendulum which is characterized by two characteristic times – the period Ω^{-1}, and the damping time (the inverse of its damping coefficient, η^{-1}). Whichever of these times is the shortest determines the system kinetics [25]. Experiments demonstrate a slowing down of slips for a narrow lubricant film, often interpreted as a strong increase of its viscosity. We showed that the slip slowing may be explained with the EQ model, if the film is inhomogeneous and consists of domains with different static thresholds. Moreover, this conclusion remains valid for a nonrigid slider as well.

In the previous work [3] devoted to the EQ model, the following conclusions were stated: in order to describe the stick-slip to smooth sliding transition in agreement with experiments, the system must (i) be two-dimensional, (ii) include interaction between the contacts, (iii) include some chaotic features (either in positions of contacts or/and in the initial configuration), and (iv) incorporate aging. In the present work, we prove that in fact items (i) and (ii) are not crucial; instead, the model must incorporate the distribution of thresholds $P_c(f_s)$ (items (i)–(iii) just act to produce this distribution). As for aging of contacts, it is still important in order to describe the dependence of friction kinetics on the driving velocity v_d; this question deserves further detailed study.

Among other important questions which were not studied yet within our model, we should mention: (i) the role of temperature, (ii) incorporation of the elastic deformation of the slider, (iii) investigation of the sliding interface in order to calculate (or to extract from experiments) the distribution $P_c(f_s)$, and (iv) the study of the distribution of delay times as well as the mechanism of contact aging (for example, if the lubricant is locally melted because of sliding, τ_f corresponds to the time for nucleation and growth of solid grains in the liquid lubricant). These questions are deferred to future studies.

Acknowledgements

We wish to express our gratitude to M. Peyrard and M. Urbakh for helpful discussions. O.B. acknowledges the hospitality of SISSA and ICTP in Trieste, and the partial support of the Central European Initiative. This project was supported by the Italian National Research Council (CNR) through ESF Eurocore/FANAS/AFRI, and by the Italian Ministry of University and Research, through PRIN/COFIN 20087NX9Y7.

References

[1] B.N.J. Persson, *Sliding Friction: Physical Principles and Applications*, Springer-Verlag, Berlin, 1998.
[2] O.M. Braun and A.G. Naumovets, Surf. Sci. Reports 60 (2006) p.79.
[3] O.M. Braun and J. Röder, Phys. Rev. Lett. 88 (2002) p.096102.
[4] J. Klein, Phys. Rev. Lett. 98 (2007) p.056101.
[5] H.-W. Hu, G.A. Carson and S. Granick, Phys. Rev. Lett. 66 (1991) p.2758.

[6] P.A. Thompson, M.O. Robbins and G.S. Grest, Israel J. Chem. 35 (1995) p.93.
[7] L. Bureau, Phys. Rev. Lett. 104 (2010) p.218302.
[8] I.F. Lyuksyutov, A.G. Naumovets and V.L. Pokrovsky, *Two-Dimensional Crystals*, Academic Press, Boston, 1992.
[9] R. Burridge and L. Knopoff, Bull. Seismol. Soc. Am. 57 (1967) p.341.
[10] O.M. Braun and E. Tosatti, Europhys. Lett. 88 (2009) p.48003.
[11] J.M. Carlson and J.M. Langer, Phys. Rev. Lett. 62 (1989) p.2632.
[12] Z. Olami, H.J.S. Feder and K. Christensen, Phys. Rev. Lett. 68 (1992) p.1244.
[13] B.N.J. Persson, Phys. Rev. B 51 (1995) p.13568.
[14] A.E. Filippov, J. Klafter and M. Urbakh, Phys. Rev. Lett. 92 (2004) p.135503.
[15] Z. Farkas, S.R. Dahmen and D.E. Wolf, J. Stat. Mech. Theory Exp. (2005) p.06015.
[16] O.M. Braun and M. Peyrard, Phys. Rev. Lett. 100 (2008) p.125501.
[17] O.M. Braun and M. Peyrard, Phys. Rev. E 82 (2010) p.036117.
[18] T. Baumberger and C. Caroli, Adv. Phys. 55 (2006) p.279.
[19] A.M. Stoneham, Solid State Commun. 24 (1997) p.425.
[20] K.H. Lau and W. Kohn, Surf. Sci. 65 (1977) p.607.
[21] O.M. Braun, M. Peyrard, V. Bortolani, A. Franchini and A. Vanossi, Phys. Rev. E 72 (2005) p.056116.
[22] J. Klein and E. Kumacheva, J. Chem. Phys. 108 (1998) p.6996.
[23] E. Kumacheva and J. Klein, J. Chem. Phys. 108 (1998) p.7010.
[24] L.D. Landau and E.M. Lifshitz, *Theory of Elasticity*, Pergamon Press, Oxford, 1970.
[25] A.D. Berman, W.A. Ducker and J.N. Israelachvili, Langmuir 12 (1996) p.4559.